Engineering Science & Technology
http://ojs.wiserpub.com/index.php/EST/

UNIVERSAL WISER PUBLISHER

Research Article

Multidisciplinary Optimization in Helical Grooved Tubes for Heat Transfer Enhancement

Shamoon Jamshed

Pakistan Navy Engineering College, Karachi, Pakistan
Email: shamoonjamshed@gmail.com

Received: 22 April 2021; **Revised:** 21 June 2021; **Accepted:** 3 July 2021

Abstract: Optimization in engineering is a significant tool for selecting the best fit when several design variables are present. It helps in determining the optimum through a combination of a set of design variables with objective functions subject to certain constraints. In the design of heat exchangers too, where tremendous research is going on to optimize its effectiveness, certain efforts are being done to improve the quality of the inner tube, shell, or plate design. In this respect, surface enhancement has been actively researched in recent decades. This sort of augmentation is usually dominant on the tube side. It has been seen that the study is greatly conducted in the past experimentally, but numerical studies are limited to determine friction factor or Nusselt number. Only a few discussed an important factor called entropy generation minimization. In this paper, with the optimization in view, the design is based on multiple disciplines. That is, first a numerical study is performed on the helically grooved tubes to examine the thermal enhancement factor. Numerical results are initially validated with published experimental results. The optimized tube is then selected based on the D-optimal design for the thermal enhancement factor and finally, the entropy minimization study concerning the Reynolds number is conducted on the optimized tube. It is observed that the tube with the greatest number of grooves, the maximum depth, and the least pitch performs the best. However, the optimum Reynolds number is at the point where the tube has the least entropy generated as compared to the smooth tube.

***Keywords*:** optimization, D-optimal design, computational fluid dynamics, grooved tube, friction factor, nusselt number, reynolds number, heat exchanger

List of symbols

Di	Internal diameter of tube [m]
Do	Outer diameter of the tube [m]
f	Friction factor, [-]
g	Acceleration due to gravity, [m/s^2]
h	Enthalpy [J/kgK]
k	Turbulent kinetic energy [J/kg]
L	Length of the tube [m]

DOI: https://doi.org/10.37256/est.222021888

Nu	Nusselt number [-]
Pr	Prandtl number [-]
Re	Reynolds number [-]
T	Temperature [K]
V	Velocity [m/s]
Δp	Pressure gradient [Pa/m]
q''	Heat flux [W/m^2]
$y+$	Dimensionless wall normal distance [-]

Greek letters

λ	Thermal conductivity [W/mK]
η	Thermal enhancement factor
μ	Absolute viscosity [kg/ms]
μ_t	Turbulent viscosity [kg/ms]
ρ	Density [kg/m^3]
ω	Specific dissipation rate [1/s]

Subscripts

avg	average
f	fluid
loc	local
o	outer
ref	reference
w	wall
t	turbulent

1. Introduction

Optimization is now a frequently used tool in engineering design. Under a certain set of variables and constraints, optimization is usually done by defining a function of an output variable and thereby determining its maximum or minimum or say the optimized point. Consequently, with analyses in engineering, optimization tools help in scenarios where a designer has to pick among many design variables. The optimization could be of cost, throughput, or efficiency. Similarly, in heat exchangers, optimization is performed by modifying certain parameters, such as the number of passes, shell or tube diameter, material properties, tube wall thickness, the length of tubes, baffle spacing, pressure, or temperature.

The performance can also be enhanced by enhancing the available surface area. Earlier, the heat enhancement study in finned/grooved tubes has been majorly conducted experimentally by computing Nusselt number and friction factor in smooth tubes. To a narrow extent, some numerical studies have also been performed by analyzing tubes' performance based on only these two parameters. However, from a thermodynamics point of view, flow effectiveness will be useful if there is a minimum loss of available work and thus a minimum entropy production rate. In the analyses conducted earlier, less literature is available that focused on the entropy minimization of the grooved tubes.

Concerning experimental study on groove tubes, a study is found in the literature by Michael Jensen and Vlakancic [1], in which the effect of fin height and depth in helical finned tubes is analyzed. The Reynolds number is varied from 10,000 to 90,000. A criterion for determining the Nusselt number and the friction factor is established and it is found that for shortfin height the friction suffers a long transition until the flow becomes turbulent in the finned region. Webb et al [2] determines different correlations for friction and Stanton number and discuss the regression curves with the behavior

predicted by roughened tubes. Mainly, his research work is based on Sabersky and Dippery's study on roughened tubes [3]. Gregory's study [4] is more comprehensive and has almost been cited in every study of helical finned tubes. His study focuses on different variations of tube design, in particular the depth and pitch. Aroonrat's research [5] comprises a more simplified analysis with four helical grooved tubes with Reynolds number 4000-10000. Among the tubes examined, the tube with the lowest pitch of 12.7 mm gives the highest Nusselt values and similarly the highest friction factor in comparison with the smooth tube.

In numerical studies, less amount of research on the helical tubes is found. The study of Kim et al [6] is novel in the way that they utilize a Finite Element Method (FEM) technique with the simplification in numerical modeling of the grooved tube. The effect of heat transfer and friction factor on the helix angle is analyzed and discussed. Piotr [7], inspired by the same modeling technique as used by Kim [6], analyzes the design of the helical finned tube using CFD. The author finds that the tube with a 70º helix angle gives the lowest entropy at optimum Reynolds number of 60,000. A modified analysis is done by Jamshed et al [9] including the comparison of a few tubes' data from the experiment [5]. It is found that the Nusselt number and friction factor are in good agreement and lie within a difference of 5% from experimental data. With regard to the optimization of grooved tubes, few papers are found mentioning the optimization of heat transfer in heat exchangers like H. Bas [10], Dastmalchi [11], and Ji-Hyun Mun [12]. The study by Halit Bas [10] is done using the Taguchi method on a tube with a twisted tape insert. He varies the clearance ratio, twist ratio, and Reynolds number while Nusselt number and pressure drop are determined as output. It is found that heat transfer augments with the decrease of twist ratio and the clearance ratio but with the increase in Reynolds number. Pressure drop decreases with twist and clearance ratio with regard to an increase in Reynolds number. Much closer work to the grooved tubes is done by Dastmalchi, who applies the Particle Swarm Optimization (PSO) technique and finds the optimum thermal enhancement factor. A similar kind of work is done by Ji-Hyun Mun [12] on the internally heated regenerator and its performance is optimized using ½ fractional Design of Experiment (DoE) optimization scheme. The rate of regeneration and its effectiveness are determined as output variables. It is found that its effectiveness is mostly affected by the regenerator air velocity.

Earlier, the work has been either done with respect to the optimization of the thermal enhancement factor only or entirely focused on minimizing the entropy generation rate. For a complete engineering design analysis, both the thermal enhancement factor and minimization of the entropy generation rate are crucial. Therefore, in this article, the thermal enhancement factor is examined numerically based on D-optimal design, and then the entropy analysis is done on the optimized geometry. This analysis was performed by examining the ratio of the entropy generation rate between the grooved and smooth tubes. The Reynolds number at which the minimum entropy generation rate is obtained is considered as the optimum Reynolds number for that tube.

2. Experimental setup

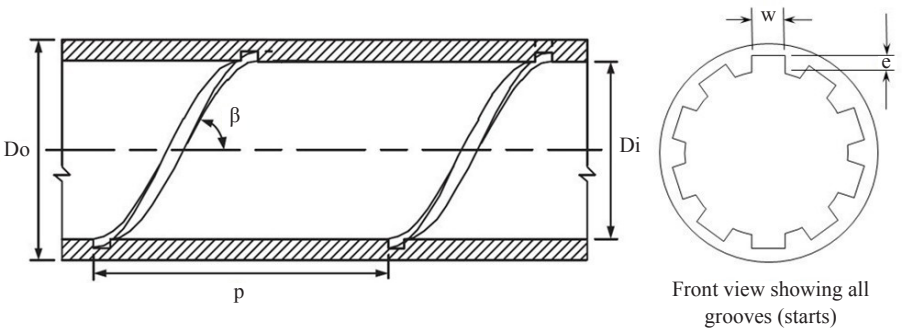

Do: Outer diameter	e: Groove depth
Di: Inner diameter	β: Helix angle
w: Groove width	p: Axial pitch length

Figure 1. The grooved tube geometry cut-away view with the nomenclature

In the initial analysis, the results are compared with an experimental study on the grooved tube by Aroonrat et al [5]. The 2 m tube is made up of Steel MS 304. For temperature measurements, T-type thermocouples are pasted on the tube surface. Water is used as a working fluid with an average temperature of 25ºC. Pressure measurement is done by mounting transducers across the length of the tube. The terminology of different geometric parameters is provided in Figure 1.

3. Numerical analysis

3.1 *Governing equations*

The numerical validation with the experimental work of Aroonrat [5] is performed for the different sets of tubes. Before discussing the meshing details and parameters used in the study, it is imperative to mention here the basic equations used in Computational Fluid Dynamics (CFD), i.e., the time-averaged equations of continuity, the incompressible momentum equation, and the energy equation. These are mentioned from Equations (1) to (3),

$$\frac{\partial \rho}{\partial t} + \rho \nabla . \bar{\boldsymbol{V}} = 0 \tag{1}$$

where $\boldsymbol{V} = \{u, v, w\}$.

Conservation of momentum equation and the energy equation are given as,

$$\frac{\partial \rho \bar{\boldsymbol{V}}}{\partial t} + \nabla . (\rho \overline{\boldsymbol{V}\boldsymbol{V}}) = -\nabla P + \nabla . (\bar{\tau}) + \rho \boldsymbol{g} \tag{2}$$

$$\frac{\partial \rho \bar{\boldsymbol{e}}}{\partial t} + \boldsymbol{V} . \nabla p = -\nabla . (k \nabla T) + \nabla . (\bar{\boldsymbol{V}} \overline{\tau_{ij}}) \tag{3}$$

To solve the turbulent flow quantities, the *k*-*ω* Shear Stress Transport (SST) model is used. The robust model is selected since it incorporates the *k*-*ε* model outside the boundary layer and *k*-*ω* standard within the boundary layer. The only requirement for using this model is that the *y*+ value should be less than 1 in the viscous sub-layer region of the turbulent boundary layer (see Ref [13]).

3.2 *Data reduction*

The Reynolds number for tube flow is based on the inner diameter of the plain pipe and its equation is given as

$$Re = \frac{\rho u D_i}{\mu} \tag{4}$$

Also, the performance of the tubes is examined taking friction factor, the Nusselt number, thermal enhancement factor, and entropy generation rate and into account. The equations of these terms are provided in Equations (5) to (10).

$$f = \frac{2 \Delta p D_i}{L \rho u^2} \tag{5}$$

where Δp gives the drop in pressure occurring along the length of the tube.

The average heat transfer coefficient can be computed from the following formula:

$$h_{avg} = \frac{\dot{Q}}{A_i (T_{avg,wi} - T_{avg,f})} \tag{6}$$

where $\dot{Q}$ is the heat provided to the outer wall, A_i is the inner-wall surface area of the tube. $T_{avg,\ wi}$ is the mean temperature of the inner wall. In CFD computations, it is found by taking the area-weighted average of each cell of the inner wall. The heat flux that is applied on the outer wall and other boundary conditions are shown in Figure 2.

The Nusselt number can be given as (based on internal diameter),

$$Nu = \frac{h_{avg} D_i}{\lambda_f} \tag{7}$$

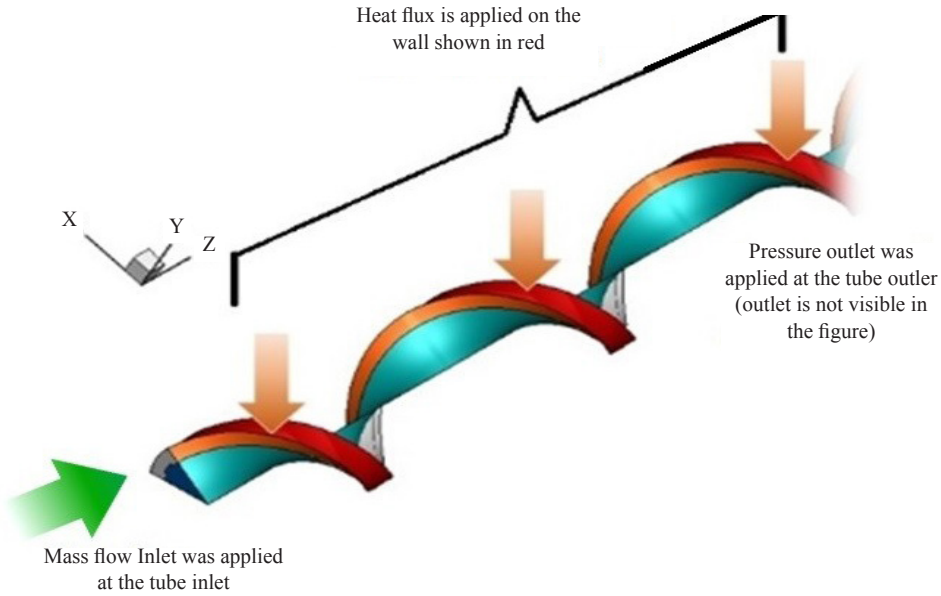

Figure 2. A sketch of the computational model of the tube showing the application of heat flux on the outer wall and other boundary conditions

As a standard practice, the heat transfer enhancement is determined for enhanced surfaces using the thermal enhancement factor. The equation for thermal enhancement factor η is given below [4], [5], [7] and [8] :

$$\eta = \frac{Nu / Nu_o}{f / f_o} \tag{8}$$

The subscript 'o' is for the smooth tube. The value of η, if greater than unity, implies that a design is favorable in terms of heat transfer enhancement.

In the advanced thermodynamics texts, like that of Bejan [14]-[17], the generation of entropy has been formulated using Equation (9).

$$\dot{S}'_{gen} = \frac{\dot{q}'(T_w - T_b)}{T_b^2} + \frac{\dot{m}}{\rho T_b}\left(-\frac{dP}{dz}\right) \tag{9}$$

The entropy generation ratio S_R has been defined as

$$S_R = \frac{\dot{S}''_{gen}}{\dot{S}''_{gen,O}} \tag{10}$$

where the subscript '*o*' is for the smooth tube.

3.3 *Mesh generation method*

The grooved tube used for analysis had an outer diameter of 9.5 mm while the inner (grooveless) diameter of 7.1 mm and is referred from Aroonrat [5]. The axial length is 2 m. The number of starts (the number of grooves appearing in cross-section) is 10. Creating mesh for such geometry is a challenging task. The present approach is inspired by the techniques of mesh previously used by Jensen and Vlakanic [1], Kim [6], and Piotr [7]. The grid is created by making a wedge-shaped element with a sector angle of 36. This provided the advantage of modeling rotational periodicity. Regions of solid and fluid are then modeled by copying edges by rotating and translating the base wedge-shaped geometry. The process is repeated several times until the length of the tube 2 m is achieved. An interface is also made between solid and fluid zones. The mesh contains mostly hexahedral cells but in the middle of the tube (near the axis), they are of prismatic shape. The mesh is shown in Figure 3.

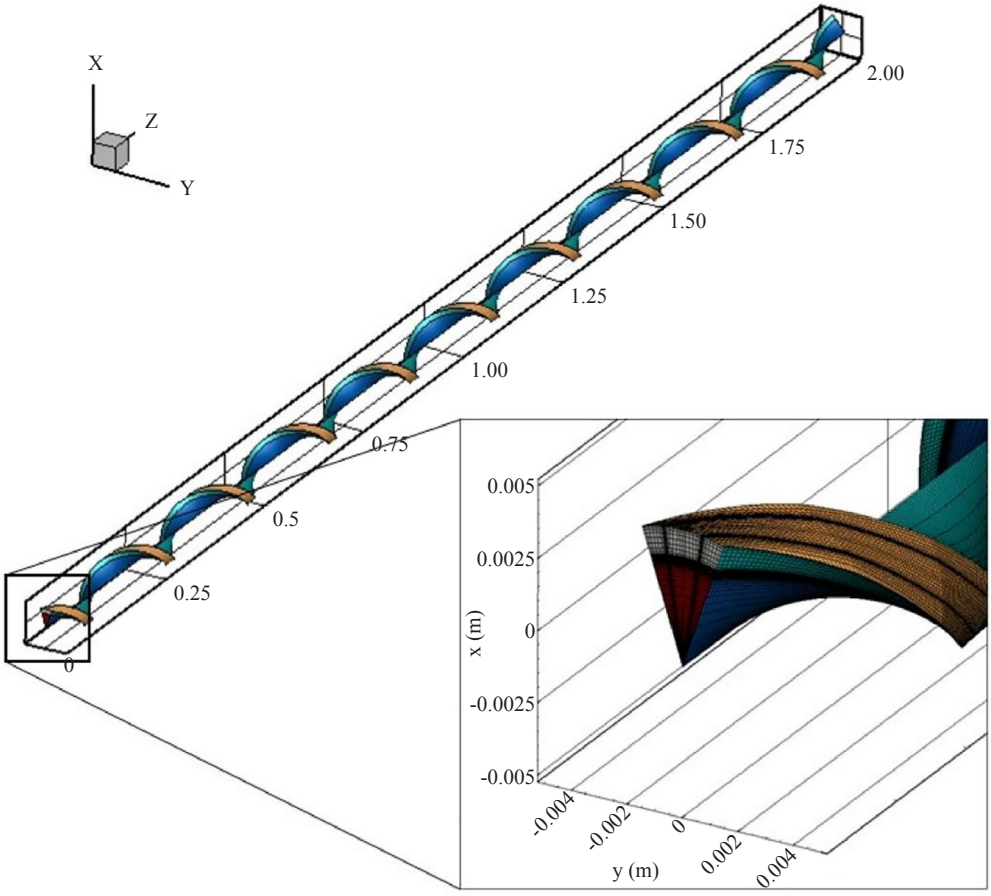

Figure 3. Three-dimensional grid view of helical grooved tube geometry with mesh details in insert

3.4 *The grid independence study*

For the grid independence study, six different geometries with different mesh sizes are constructed and results are discussed. The details are given in Table 1. The mesh is kept fine near the wall to cater for viscous effects and to ensure $y+ < 1$. In each case, the Nusselt number and axial velocity are monitored and are mentioned in Table 1. It can be seen that the variation diminishes after three levels of refinement with less than 0.5% difference in the case of velocity, while it is much lesser for the last two levels in the case of the Nusselt number (about 0.05%). Therefore, for validation with experimental data, mesh level V is selected. The surety of $y+$ is also done by plotting $y+$ versus shear velocity (u_τ) graph as shown in Figure 4. The last three levels have enough cells in the viscous sub-layer and therefore, based on the limitation of available resources, the mesh level V is considered reasonable.

Table 1. Details of the parameters for the grid convergence study

Refinement level	Total number of cells	First cell height distance placed in the grid (mm)	Velocity at the outlet (m/s)	Averaged Nusselt number
I	595272	0.13	1.5500	108.01
II	1059356	0.01	1.5850	105.35
III	1529612	0.01	1.5918	103.52
IV	2566642	0.001	1.5925	99.27
V	3387852	0.001	1.5938	99.32
VI	4430268	0.001	1.5952	99.32

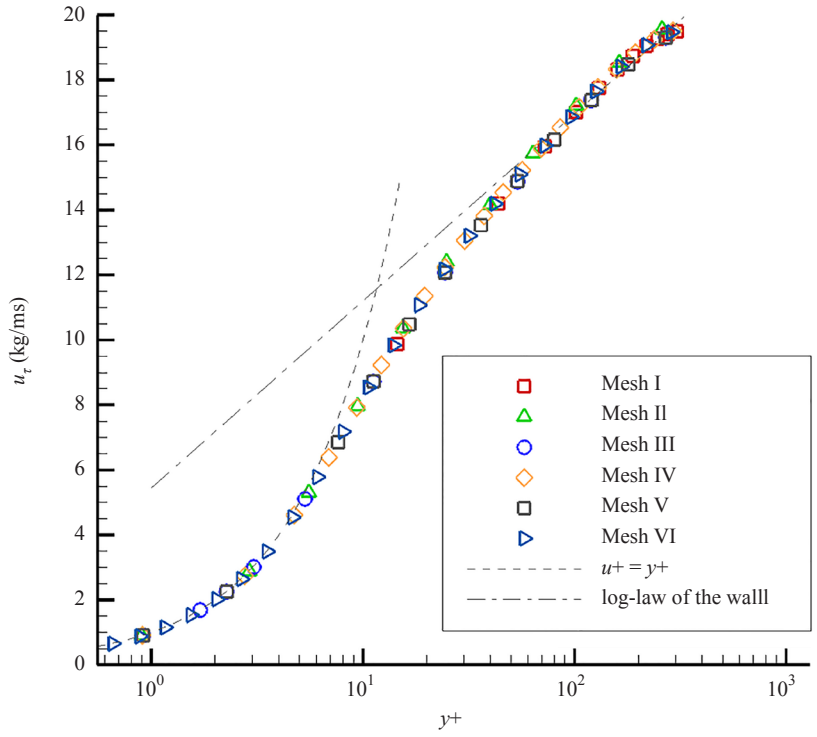

Figure 4. $y+$ versus u_τ curve for six different levels of mesh sizing

4. Results and discussion

4.1 *Validation with experimental data*

4.1.1 *Validation of helical groove tubes with 203 mm and 254 mm pitch length (GT08 and GT10)*

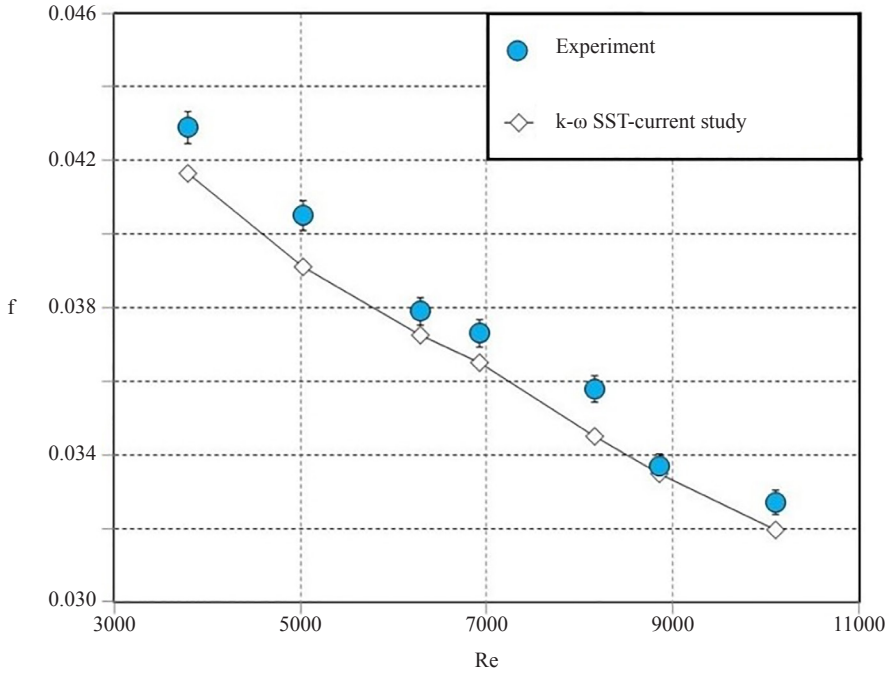

Figure 5. Comparison of friction factor with experimental data as a function of Reynolds number for GT08 (203 mm pitch length)

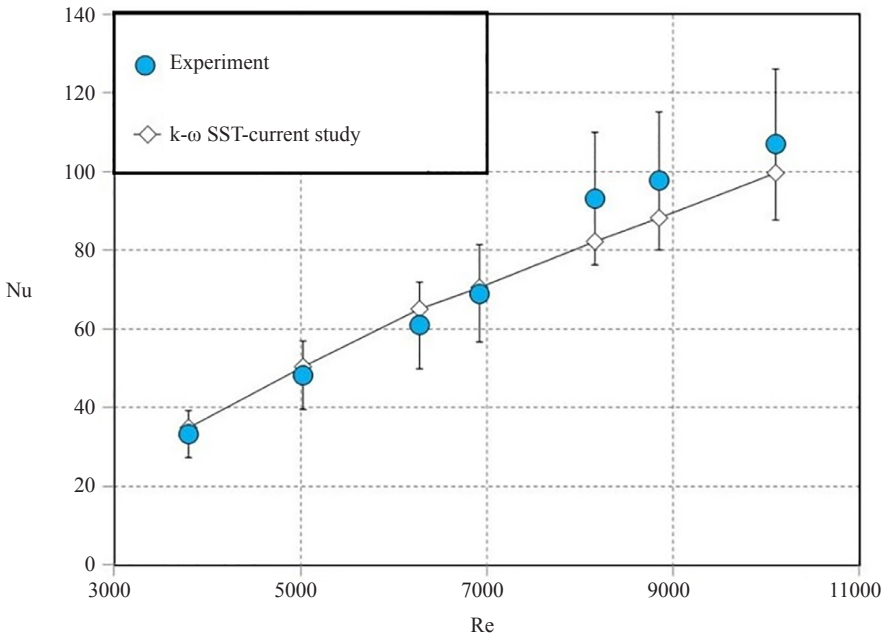

Figure 6. Comparison of Nusselt number with experimental data as a function of Reynolds number for GT08 (203 mm pitch length)

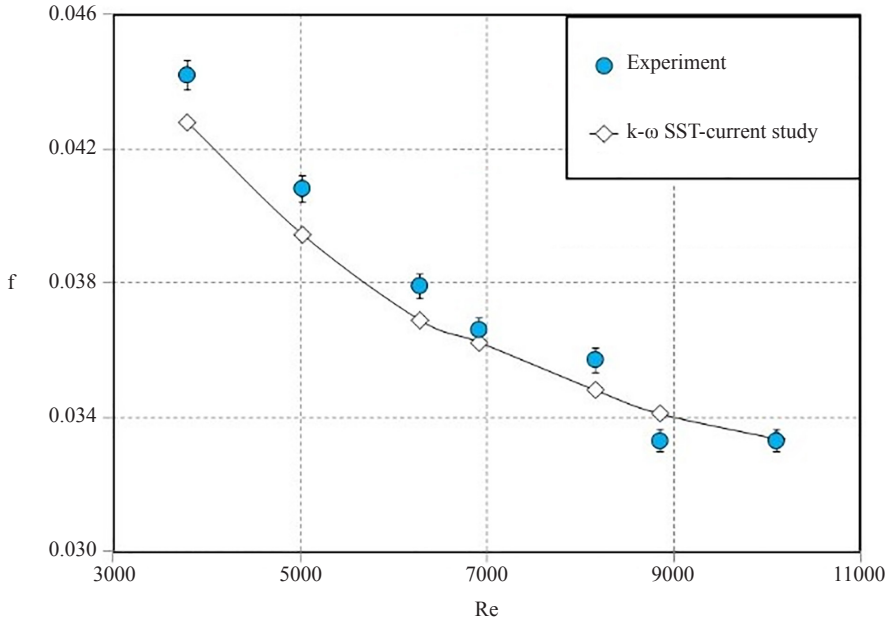

Figure 7. Comparison of friction factor with experimental data as a function of Reynolds number for GT10 (254 mm pitch length)

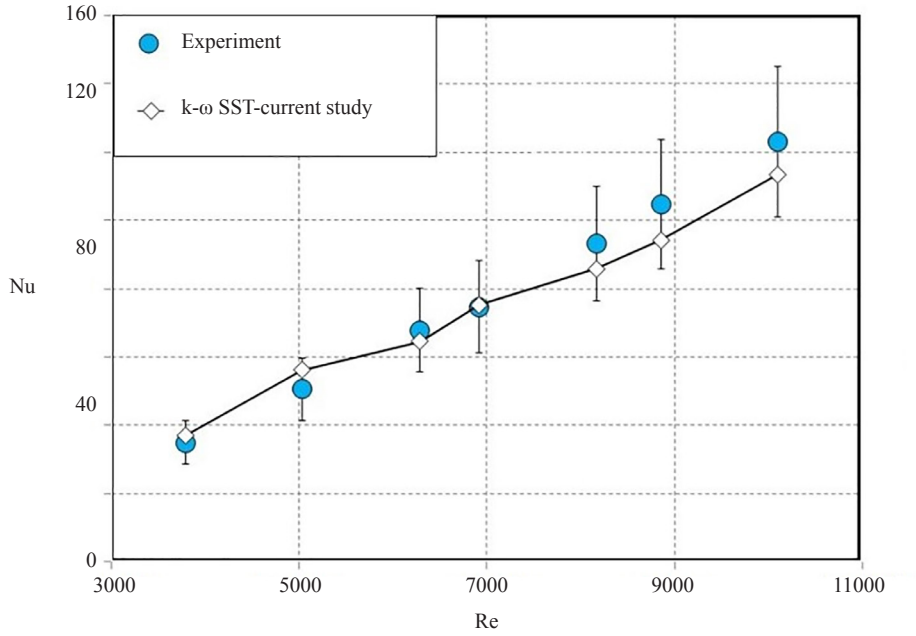

Figure 8. Comparison of Nusselt number with experimental data as a function of Reynolds number for GT10 (254 mm pitch length)

Validation of the CFD results is done by comparison with Aroonrat et al's [5] experimental data. Two parameters, viz. friction factor and Nusselt number are compared. Figure 5 to Figure 8 show the plots for the friction factor and the Nusselt number for the helical tubes with 203 mm and 254 mm pitch length respectively. The average error (over the Re range) in the case of friction factor is within 2% for both cases. In the case of the Nusselt number, the difference of CFD results with the experiment is also low (about 7% on average over the Re range), and it also lies within the uncertainty limit of ±18% of experimental data. After the satisfactory agreement with the experiment, further tubes are studied

based on the D-optimal design technique.

Table 2 summarizes the design matrix. In the first iteration, a design matrix is created using the quadratic-plus-interaction model, since the interaction terms, the squared-terms and individual effect of the factor-terms, i.e., the pitch length (p_L), the number of starts (Ns), and the groove depth (e) are considered important. By getting this matrix, the CFD analysis is performed on all the tubes to get η_{computed}. When a response surface is applied for obtaining $\eta_{\text{predicted}}$, it gives a p-value that is greater than 0.1 for squared terms of Ns, p_L, and e. This means that the model is not suitable as optimized. In the second iteration, the linear-plus-interaction model is selected and CFD is performed to get η_{computed}. By again repeating the response surface method to get $\eta_{\text{predicted}}$, the p-value is 0.05 for all of the terms. Therefore, this model is chosen for further analysis. A value of 0.05 or less specifies the rejection of the null hypothesis. It tells about the hypothesis testing of the equal fitting of the computed model and predictive model. Thus, if the p-value is less than the significance level (usually 0.05) then the predicted model (or model coefficients) are significant where the null hypothesis indicates that they are not significant. After the analysis, the predicted values are very close to the computed values. Statistical analysis from Minitab shows R^2 value of 0.995 while the p-value is as low as 0.005. Thus, the model of linear-and-interaction terms is statistically acceptable. The predicted model has the following correlation:

$$\eta_{predicted} = 0.7538 + 0.1007N_s + 0.0521e - 0.1047P_L + 0.0701N_s \times e - 0.0579N_s \times p_L + 0.1058e \times p_L \quad (11)$$

Table 2. The design matrix created by the D-optimal design using an interaction model

Ns	e	p_L	η_{computed}	$\eta_{\text{predicted}}$
-1	-1	1	0.4997	0.5186
-1	-1	-1	0.8425	0.8237
-1	1	1	0.7131	0.6942
1	-1	1	0.4828	0.4640
1	1	1	0.8820	0.9198
-1	1	-1	0.5573	0.5762
1	-1	-1	0.9819	1.0008
1	-1	1	0.4828	0.4640
-1	-1	1	0.4997	0.5186
1	1	-1	1.0524	1.0336
-1	-1	-1	0.8425	0.8237
-1	1	-1	0.5573	0.5762
1	-1	-1	0.9820	1.0008
-1	1	1	0.7131	0.6942
1	1	-1	1.0524	1.0336

With this experimentation, it is not difficult to judge that all of the designs that have η less than 1 are least significant from the heat enhancement point of view. Although groove tubes are meant to be advantageous only if they are better than the smooth tube, a value of 0.9 can still be advantageous thermally if a high friction factor due to groove formation is compromised to some extent. The optimized tube has the largest number of grooves, the least pitch, and

maximum groove depth with η = 1.05. Figure 9 shows the margins between the CFD and the predicted response. It shows that the difference lies under 5%, which is quite a good estimate.

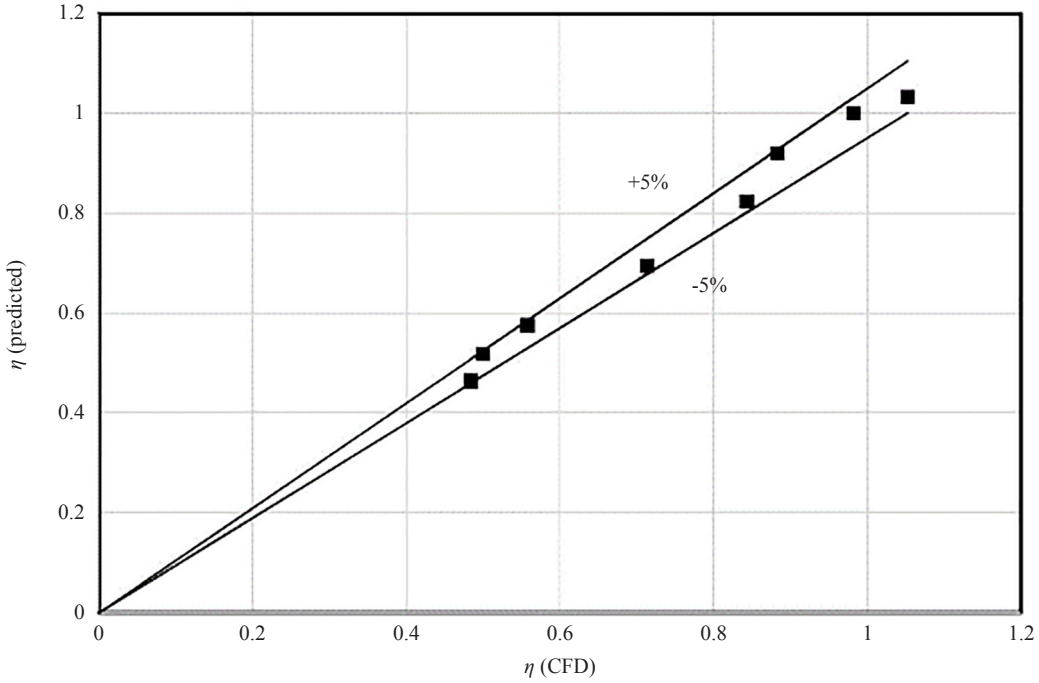

Figure 9. A graph showing the difference between CFD and response surface predicted values showing a difference of ±5%

It is obvious that the extreme conditions give the maximum output, but the relations such as Gregory [4] also support this kind of result. A similar finding is also observed by Jamshed et al [9], where the lowest pitch of 2-inch length gives the highest thermal enhancement factor among the tested tubes of varying pitch lengths. Therefore, it is justified to use the optimum tube for further analysis on the entropy.

4.2 *Entropy-generation-rate minimization*

Adrian Bejan [14]-[17], presented the idea of minimizing entropy-generation-rate with the perspective of heat transfer and fluid dynamics. In the case of devices involving heat transfer, a trade-off lies between heat transfer irreversibility. This trade-off can be described using the entropy-generation-rate ratio. The entropy ratio is the ratio of entropy generated in the case of augmented tubes and the entropy in the case of smooth tubes and is given in Equation (10). Fewer studies, like that of Piotr, are found for studying entropy in grooved tubes numerically while some sources discuss the entropy minimization based on axial groove shape or protrusion over a surface like Ramadhan [23] and Nianben et al [24].

Bejan [14]-[17] mentions a curve for entropy generation ratio vs. Reynolds number and specifies a point where minimum entropy is generated. The optimum point is at a location where the irreversibility due to heat and friction becomes equal. It can be seen in Figure 10. After this point, moving right along the curve is the region where pressure effects (and hence friction) dominates while moving left of the optimum point is the region where thermal effects are dominant. This concept has also been discussed in texts like Herwig and Kock [18], Herwig [19], and Mahian et al [20].

Based on the same analogy, a curve for entropy ratio S_R can also be plotted. This ratio comprises the entropy generated due to augmentation to the entropy generated due to the smooth tube. The optimum point is the point where S_R is unity. Therefore, the Reynolds number at which this ratio occurs is the optimum Reynolds number for the particular augmented tube.

The entropy curve obtained at different Reynolds numbers for the optimized tube is shown in Figure 11. The curve shows that the entropy ratio drastically changes after the Reynolds number of 8000. The optimum point comes when S_R becomes 1. This point lies at nearly Re = 5000. It can be seen that simulating flow in a tube, which can give a higher thermal enhancement factor, has an optimized S_R at a much lower Reynolds number. However, at this S_R, a lower Reynolds number could lead to lower η and since the S_R again increases with further lowering Re, the performance would be inferior and it would become more advantageous to use a smooth tube than a grooved tube if Re is lower than 5000.

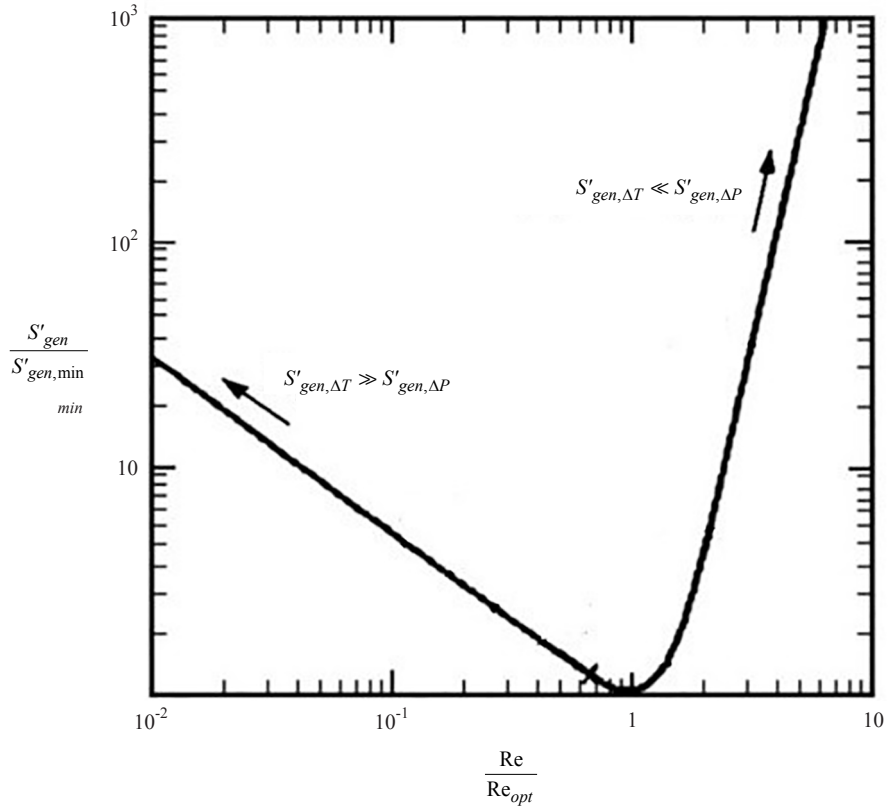

Figure 10. Optimization curve showing the relative entropy generation ratio versus Reynolds number ratio, Bejan [14]-[17]

A correlation is developed by matching a curve of 2nd order with the present results. The equation of the curve is given in Equation (12). This correlation can be used for a range of Reynolds numbers for a tube with similar dimensional parameters.

$$S_R = 1.188 \times 10^{-7} Re^2 - 0.001152 Re + 3.773 \tag{12}$$

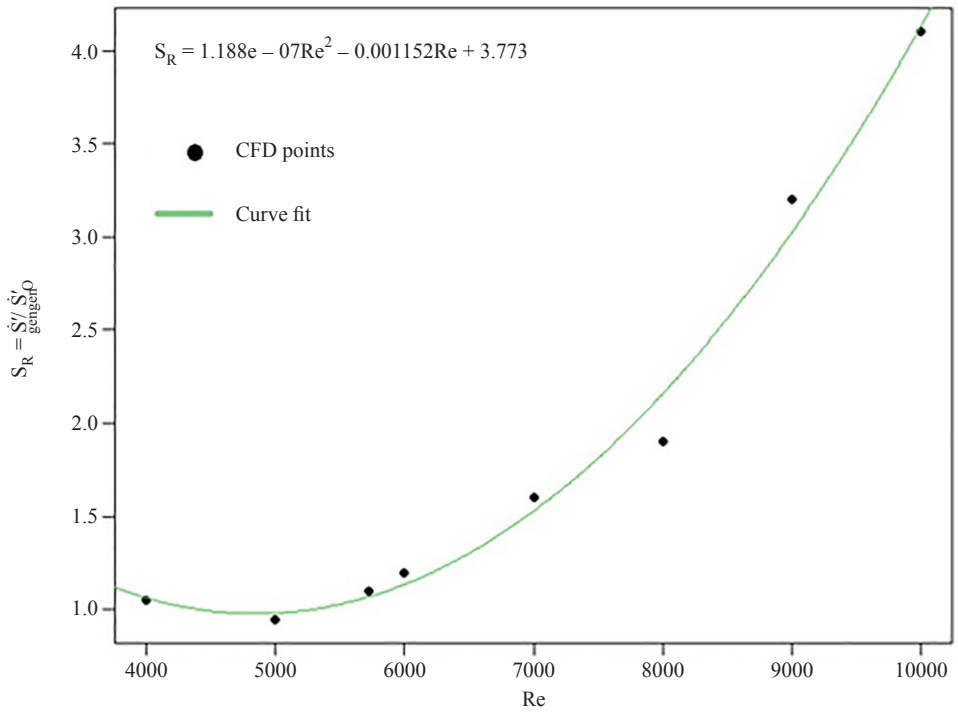

Figure 11. The entropy ratio curve and the correlation shown for the tube with Ns = 30, e = 0.5 mm, and p_L = 25.4 mm (1 inch)

5. Conclusions

It has been seen in literature that limited data is available for a complete analysis of groove tubes. This limited analysis encircles the thermal enhancement factor only or the entropy-generation-minimization effect. However, just a few researchers discussed both topics in detail. For a complete engineering design analysis, both the thermal enhancement factor η and the minimization of the entropy generation rate S_R are crucial. Therefore, in this article, the thermal enhancement factor is examined numerically based on the D-optimal design and then the minimum entropy generation rate is analyzed in detail on the optimized geometry. Based on the D-optimal design analysis, the objective function (which is the thermal enhancement factor η) is optimized. The analysis shows that η is found optimum for the tube with Ns = 30, groove depth e = 0.5 mm, and pitch length p_L = 1 inch. Further, this optimum tube is examined with the analysis of the ratio of the entropy generation rate between the grooved and the smooth tube. The Reynolds number at which the minimum entropy generation rate is obtained is considered as the optimum Reynolds number for that tube. The rationale is to conclude the optimum Reynolds number at a point where S_R equals unity. For the optimum tube found, the S_R is found to be unity at Reynolds number 5,000. A correlation is developed for S_R indicating that it can be used for determining the optimum entropy curve for a tube with similar design configurations in the specified Reynolds number range.

Acknowledgements

The provision of the computational facility of the PNEC of the National University of Sciences & Technology for performing this work is highly acknowledged by the author.

Conflict of interest

The author declares that there is no conflict of interest regarding the publication of this paper.

References

[1] M. K. Jensen, and A. Vlakancic, "Technical note experimental investigation of turbulent heat transfer and fluid flow in internally finned tubes," *International Journal of Heat and Mass Transfer*, vol. 42, no. 7, pp. 1343-1351, 1999.

[2] R. L. Webb, R. Narayanamurthy, and P. Thors, "Heat transfer and friction characteristics of internal helical-rib roughness," *Journal of Heat Transfer*, vol. 122, no. 1, pp. 134-142, 2000. Available: https://dx.doi.org/10.1115/1.521444.

[3] D. F. Dipprey, and R. H. Sabersky, "Heat and momentum transfer in smooth and rough tubes at various Prandtl numbers," *International Journal of Heat and Mass Transfer*, vol. 6, no. 5, pp. 329-353, 1963. Available: https://dx.doi.org/10.1016/0017-9310(63)90097-8.

[4] G. J. Zdaniuk, L. M. Chamra, and P. J. Mago, "Experimental determination of heat transfer and friction in helically-finned tubes," *Experimental Thermal and Fluid Science*, vol. 32, no. 3, pp. 761-775, 2008. Available: https://dx.doi.org/10.1016/j.expthermflusci.2007.09.006.

[5] K. Aroonrat, C. Jumpholkul, R. Leelaprachakul, A. S. Dalkilic, O. Mahian, and S. Wongwises, "Heat transfer and single-phase flow in internally grooved tubes," *International Communications in Heat and Mass Transfer*, vol. 42, pp. 62-68, 2013. Available: https://dx.doi.org/10.1016/j.icheatmasstransfer.2012.12.001.

[6] J.-H. Kim, K. E. Jansen, and M. K. Jensen, "Simulation of three-dimensional incompressible turbulent flow inside tubes with helical fins," *Numerical Heat Transfer, Part B: Fundamentals*, vol. 46, no. 3, pp. 195-221, 2004. Available: https://dx.doi.org/10.1080/10407790490449499.

[7] P. Jasinski, "Numerical optimization of flow heat ducts with helical micro-fins, using Entropy Generation Minimiza-tion (EGM) method," in: *Recent Advances in Fluid Mechanics and Heat & Mass Transfer,* WSEAS Press, 2011, pp. 47-54.

[8] A. Tiwari, and S. Yavuzkurt, "A comparative study of performance of low Reynolds number turbulence models for various heat transfer enhancement simulations," *Journal of Heat Transfer*, vol. 141, no. 7, pp. 071902, 2019. Available: https://dx.doi.org/10.1115/1.4043305.

[9] S. Jamshed, S. Qureshi, and S. Khalid, "Numerical flow analysis and heat transfer in smooth and grooved tubes," *Wessex Transactions on Engineering Sciences, 11th International Conference on Advances in Fluid Mechanics*, vol. 105, pp. 163-174, 2016.

[10] H. Bas, and V. Ozceyhan, "Optimization of parameters for heat transfer and pressure drop in a tube with twisted tape inserts by using taguchi method," *Arabian Journal for Science and Engineering*, vol. 39, no. 2, pp. 1177-1186, 2014. Available: https://dx.doi.org/10.1007/s13369-013-0648-4.

[11] M. Dastmalchi, G. A. Sheikhzadeh, and A. Arefmanesh, "Optimization of micro-finned tubes in double pipe heat ex-changers using particle swarm algorithm," *Applied Thermal Engineering*, vol. 119 pp. 1-9, 2017. Available: http://dx.doi.org/10.1016/j.applthermaleng.2017.03.025.

[12] J.-H. Mun, D.-S. Jeon, Y.-L. Kim, and S.-C. Kim, "A study on the regeneration performance characteristics of an internally heated regenerator in a liquid desiccant system," *Journal of Mechanical Science and Technology*, vol. 30, no. 3, pp. 1343-1349, 2016. Available: https://dx.doi.org/10.1007/s12206-016-0241-3.

[13] F. R. Menter, "Two-equation eddy-viscosity turbulence models for engineering applications," *AIAA Journal*, vol. 32, no. 8, pp. 1598-1605, 1994. Available: https://dx.doi.org/10.2514/3.12149.

[14] A. Bejan, "Entropy generation minimization: The method and its applications," *Journal of Mechanical Engineering*, vol. 48, no. 8, pp. 345-355, 2001.

[15] A. Bejan, "Second-law analysis in heat transfer and thermal design", *Advances in Heat Transfer*, vol. 15, pp. 1-58, 1982. Available: https://dx.doi.org/10.1016/S0065-2717(08)70172-2.

[16] A. Bejan, "Entropy generation minimization: The new thermodynamics of finite-size devices and finite-time processes," *Journal of Applied Physics*, vol. 79, no. 3, pp. 1191-1218, 1996. Available: https://dx.doi.org/10.1063/1.362674.

[17] A. Bejan, "Theory of heat transfer-irreversible power plants," *International Journal of Heat and Mass Transfer*, vol. 31, no. 6, pp. 1211-1219, 1988. Available: https://dx.doi.org/10.1016/0017-9310(88)90064-6.

[18] H. Herwig, F. Kock, "Direct and indirect methods of calculating entropy-generation-rates in turbulent convective heat transfer problems", *Journal of Heat and Mass Transfer*, vol. 43, pp. 207-215, 2007. Available: https://dx.doi.org/10.1007/s00231-006-0086-x.
[19] H. Herwig, "The role of entropy generation in momentum and heat transfer", *Journal of Heat Transfer*, vol. 134, no. 3, pp. 031003, 2012.
[20] O. Mahian, "A review of entropy generation in nano-fluid flow," *International Journal of Heat and Mass Transferr*, vol. 65, pp. 514-532, 2013.
[21] M. Cavazzuti, *Optimization methods: From theory to design scientific and technological aspects in mechanics*. Springer, 2013.
[22] D-Optimal designs. *Chapter 267: D-Optimal designs*. NCSS, LLC, 2018, pp.1-20. Available: http://ncss.wpengine.netdna-cdn.com/wp-content/themes/ncss/pdf/Procedures/NCSS/D-Optimal_Designs.pdf.
[23] A. A. Ramadhan, Y. T. A. Anii, and A. J. Shareef, "Groove geometry effects on turbulent heat transfer and fluid flow," *Heat and Mass Transfer*, vol. 49, no. 2, pp. 185-195, 2013. Available: https://dx.doi.org/10.1007/s00231-012-1076-9.
[24] N. Zheng, P. Liu, F. Shan, Z. Liu, and W. Liu, "Turbulent flow and heat transfer enhancement in a heat exchanger tube fitted with novel discrete inclined grooves," *International Journal of Thermal Sciences*, vol. 111, no. 2, pp. 289-300, 2017. Available: https://dx.doi.org/10.1016/j.ijthermalsci.2016.09.010.